arXiv:1702.06039v1 [cond-mat.mtrl-sci] 20 Feb 2017

Doping anatase TiO_2 with group V-b and VI-b transition metal atoms : a hybrid functional first-principles study

Masahiko Matsubara,[a,c] Rolando Saniz,[b] Bart Partoens,[b] and Dirk Lamoen*[a]

We investigate the role of transition metal atoms of group V-b (V, Nb, Ta) and VI-b (Cr, Mo, W) as n- or p-type dopants in anatase TiO_2 using thermodynamic principles and density functional theory with the Heyd-Scuseria-Ernzerhof HSE06 hybrid functional. The HSE06 functional provides a realistic value for the band gap, which ensures a correct classification of dopants as shallow or deep donors or acceptors. Defect formation energies and thermodynamic transition levels are calculated taking into account the constraints imposed by the stability of TiO_2 and the solubility limit of the impurities. Nb, Ta, W and Mo are identified as shallow donors. Although W provides two electrons, Nb and Ta show a considerable lower formation energy, in particular under O-poor conditions. Mo donates in principle one electron, but under specific conditions can turn into a double donor. V impurities are deep donors and Cr shows up as an amphoteric defect, thereby acting as an electron trapping center in n-type TiO_2 especially under O-rich conditions. A comparison with the available experimental data yields excellent agreement.

1 Introduction

TiO_2 is an important material in the field of renewable energy applications, and well-known as an efficient photocatalyst used e.g. for the hydrogen production by water splitting.[1] In addition, TiO_2, more specifically the anatase phase, is suitable for producing novel materials by doping with transition metal (TM) atoms, because of their high solubility in this phase.[2] Anatase itself is a wide band gap ($\sim$3.4 eV[3]) semiconductor, which is low cost, non-toxic and chemically stable. On doping with group V-b elements Nb[4,5], Ta[6] or with W (group VI-b)[7] it becomes a good transparent conducting oxide (TCO).

Thus, TM-doped anatase is considered to be one of the promising candidates as an effective TCO to replace the currently most used but expensive indium-tin-oxide in the near future. The novelty of doped anatase is not limited to TCOs. When doped with other TM atoms, it exhibits different properties e.g. when anatase is doped with Co, it becomes a dilute magnetic semiconductor (DMS) showing ferromagnetism at room temperature.[8,9] Furthermore, V-doped anatase is a potential DMS with a giant magnetic moment[10] and Cr-doped anatase is also shown to become a DMS with a magnetization of $\sim$ 0.6 μ_B/Cr atom.[11] Doping with Mo improves the photocatalytic activity of TiO_2 [12–14] and increases the conductivity.[15]

In this paper we perform a systematic analysis of the dopant characteristics of elements from group V-b (V, Nb, Ta) and group VI-b (Cr, Mo, W) in anatase TiO_2 based on thermodynamic principles and density functional theory (DFT). These dopants have been considered before within DFT, often with the generalized gradient approximation (GGA) for the exchange-correlation functional or within the DFT+U method and with a focus on neutral impurities and their electronic properties.[16–27] However, whether an impurity becomes electrically active or rather remains inactive or even behaves amphoteric often depends on the growth conditions (e.g. the presence of native defects) and cannot directly be inferred from a DFT calculation on a neutral defect alone. A more complete picture emerges from a general thermodynamic analysis based on the defect formation energy.[28,29] Such an analysis was applied by Osorio-Guillén et al. on the V-b TM impurities in TiO_2 based on a GGA functional together with a correction scheme that accounts for the finite size of the supercell and the underestimation of the GGA band gap[17] and for Nb-doped TiO_2 a similar approach was followed in refs. 18,19. In the present work we consider both V-b and VI-b impurities and avoid an *a posteriori* correction of the band gap by using the Heyd-Scuseria-Ernzerhof (HSE) hybrid functional.[30,31]

Our work provides insight into several experimental observations. It shows that Nb, Ta and W are electron donors leading to transparent conducting TiO_2 but with different charge carrier concentrations due to the difference in defect formation enthalpy. In contrast, V will not easily donate electrons since the ionization energy is too large. Moreover we demonstrate that, depending on the actual experimental conditions, Cr acts as an amphoteric impurity and that Mo can exist as a single or double electron donor.

The paper is organized as follows. In section 2 we present the

[a] *EMAT , Departement Fysica, Universiteit Antwerpen, Groenenborgerlaan 171, B-2020 Antwerpen, Belgium*

[b] *CMT, Departement Fysica, Universiteit Antwerpen, Groenenborgerlaan 171, B-2020 Antwerpen, Belgium*

[b] *ECE, Boston University, 8 Saint Mary's Street, Boston, MA 02215, USA*

∗ Corresponding author:Dirk.Lamoen@uantwerpen.be

Table 1 Lattice constants and band gap value of anatase TiO_2 obtained by PBE and HSE along with experimental values.[3,35]

	a (Å)	c (Å)	u	E_g (eV)
PBE	3.811	9.713	0.207	2.09
HSE	3.771	9.604	0.206	3.62
Experiment	3.782	9.502	0.208	3.4

computational details for the DFT calculations (subsection 2.1) and the methodology used to calculate the defect formation energies (subsection 2.2). In section 3.1 we present the results on the formation energy of the different TM oxides considered in this work and in section 3.2 we discuss the defect formation energies and the thermodynamic transition levels. Our conclusions are given in section 4.

2 Methods

2.1 Computational details

Our DFT calculations are performed using the projector augmented wave method as implemented in the VASP code[32,33] and are spin polarized for all TM-doped systems. We treat $3p$, $3d$ and $4s$ states as valence states for Ti, V and Cr. Similarly, $4p$, $4d$ and $5s$ states are treated as valence states for Nb and Mo, whereas $5p$, $5d$ and $6s$ states are treated as valence states for Ta and W. Wave functions are expanded with a plane-wave basis set with a cutoff energy of 400 eV. We have used both the Perdew-Burke-Ernzerhof (PBE) functional[34] within GGA and the HSE hybrid functional[30,31] for the exchange & correlation energy. More specifically we used the HSE06 functional with a screening parameter of $\mu = 0.2$ Å^{-1} and a 25% mixing of Hartree-Fock exchange.

Anatase TiO_2 has a tetragonal structure with space group $I4_1/amd$ (#141). The lattice constants a and c and the internal parameter u of the anatase unit cell are optimized by both PBE and HSE. A Monkhorst-Pack k-point mesh of $7\times7\times7$ was used for the Brillouin zone integration. The obtained lattice constants along with the (indirect) band gap value (E_g) are shown together with the experimental values[3,35] in Table 1. The calculated lattice constants (both HSE and PBE) are in good agreement with the experimental results, although HSE gives a somewhat better result. The band gap value is severely underestimated (by ∼1.3 eV) in PBE, whereas HSE significantly improves the result and only slightly overestimates the experimental value by ∼0.2 eV.

Using these optimized lattice constants we construct $3\times3\times1$ tetragonal supercells including 108 atoms (36 Ti and 72 O atoms). Replacing one of the Ti atoms by a TM atom results in a dopant concentration of ∼2.8%. For this supercell a Monkhorst-Pack k-point mesh of $2\times2\times2$ was used for the Brillouin zone integration. For TM-doped TiO_2 the size of the supercell was kept fixed but the atomic positions were relaxed until forces were smaller than 0.05 eV/Å.

2.2 Formation energies and chemical potentials

The key quantity to determine the concentration, the solubility and the thermodynamic (and optical) transition levels of an impurity X in charge state q is the defect formation energy $E^f(X^q)$. For an impurity atom X (X = V, Cr, Nb, Ta, Mo or W) replacing a Ti atom it is defined by[28,29]:

$$\begin{aligned} E^f(X^q) &= E_{tot}(X^q) - E_{tot}(\mathrm{TiO_2}) + \mu_{\mathrm{Ti}} - \mu_{\mathrm{X}} \\ &\quad + q(E_v + E_F + \Delta V) + \Delta E(q). \end{aligned} \tag{1}$$

Here, $E_{tot}(X^q)$ and $E_{tot}(\mathrm{TiO_2})$ are the total energies of the supercell containing the defect X in charge state q and of the perfect crystal, respectively. μ_{Ti} and μ_{X} are the chemical potential of Ti and the impurity X respectively. The defect formation energy depends also on the chemical potential of the electrons (the "Fermi energy", E_F) and is conventionally given with respect to the valence band maximum (VBM, E_v) of the undoped system, where E_F usually ranges from the VBM to the conduction band minimum (CBM, E_c). The correction ΔV aligns the reference potential of the undoped crystal with that of the doped one and is calculated following the procedure introduced in ref. 36. $\Delta E(q)$ accounts for the electrostatic correction necessary in the case of charged defects[28]. We use the Madelung potential, as derived by Rurali and Cartoixà for anisotropic systems[37], i.e., depending on the dielectric tensor, ε, of the host material. Specifically, we write $\Delta E(q) = -\frac{q}{2}V_M(q)$, with the generalized Madelung potential given by

$$\begin{aligned} V_M(q) &= \sum_{\mathbf{R}\neq\mathbf{0}} \frac{q}{\sqrt{det\varepsilon}} \frac{\mathrm{erfc}(\gamma\sqrt{\mathbf{R}\varepsilon^{-1}\mathbf{R}})}{\sqrt{\mathbf{R}\varepsilon^{-1}\mathbf{R}}} - \frac{\pi q}{\Omega\gamma^2} \\ &\quad + \sum_{\mathbf{G}\neq\mathbf{0}} \frac{4\pi q}{\Omega} \frac{\exp(-\mathbf{G}\varepsilon\mathbf{G}/4\gamma^2)}{\mathbf{G}\varepsilon\mathbf{G}} - \frac{2\gamma q}{\sqrt{\pi det\varepsilon}}. \end{aligned} \tag{2}$$

The summations of $\mathbf{R}$ and $\mathbf{G}$ run over the direct and reciprocal lattices, respectively. γ is a suitably chosen convergence parameter and Ω is the volume of the primitive cell. The above has proven to be an excellent correction scheme for anisotropic systems.[37–39] We use the experimental values for anatase TiO_2, $\varepsilon_\infty^{\parallel} = 5.41$, $\varepsilon_\infty^{\perp} = 5.82$, and $\varepsilon_0^{\parallel} = 22.7$, $\varepsilon_0^{\perp} = 45.1$[40] Note that because of the large size of the dielectric tensor components, the electrostatic correction is rather small in the present case.

The chemical potential for Ti, and the impurity X will always be given with respect to the total energy per atom of its bulk metallic phase, e.g. $\mu_{\mathrm{X}} = E_{tot}(\mathrm{X}) + \Delta\mu_{\mathrm{X}}$. * μ_{O} is referenced to the total energy of an O atom in an O_2 molecule, $\mu_{\mathrm{O}} = 1/2E_{tot}(O_2) + \Delta\mu_O$. The chemical potentials of O and Ti should satisfy the stable growth condition for TiO_2,

$$\Delta\mu_{\mathrm{Ti}} + 2\Delta\mu_{\mathrm{O}} = \Delta H_f(\mathrm{TiO_2}). \tag{3}$$

$\Delta H_f(\mathrm{TiO_2})$ denotes the enthalpy of formation for TiO_2. Under extreme O-rich conditions, $\Delta\mu_{\mathrm{O}} = 0$. Under extreme Ti-rich conditions, the growth of Ti_2O_3 becomes favorable, because the Ti/O ratio in this compound is higher than that in TiO_2. As a result,

* For metallic Ti and X we considered the hexagonal close-packed (space group # 194) and body-centered cubic (space group # 229) structure respectively, with the exception of Cr for which we considered the CsCl structure with an antiferromagnetic ordering.

$\Delta\mu_{\mathrm{Ti}}$ is bounded by the formation of Ti_2O_3,

$$2\Delta\mu_{\mathrm{Ti}} + 3\Delta\mu_{\mathrm{O}} = \Delta H_f(\mathrm{Ti_2O_3}), \quad (4)$$

where $\Delta H_f(\mathrm{Ti_2O_3})$ denotes the enthalpy of formation for Ti_2O_3. The intersection of Eqs. (3) and (4) corresponds to the upper limit of the chemical potentials for stable TiO_2 growth, i.e. $\Delta\mu_{\mathrm{Ti}} = 2\Delta H_f(\mathrm{Ti_2O_3}) - 3\Delta H_f(\mathrm{TiO_2})$ and $\Delta\mu_{\mathrm{O}} = -\Delta H_f(\mathrm{Ti_2O_3}) + 2\Delta H_f(\mathrm{TiO_2})$. In Table 2 we summarize the PBE and HSE results for the formation enthalpy of TiO_2 and Ti_2O_3, and the values for $\Delta\mu_{\mathrm{Ti}}$ and $\Delta\mu_{\mathrm{O}}$ both for O-rich and Ti-rich conditions. The enthalpies of formation calculated by HSE are in better agreement with the experimental values[41] than those calculated by PBE.

The solubility limit of impurity X (X = V, Cr, Nb, Ta, Mo or W) is determined by the formation of the corresponding oxides i.e.

$$x\Delta\mu_{\mathrm{X}} + y\Delta\mu_{\mathrm{O}} = \Delta H_f(\mathrm{X}_x\mathrm{O}_y). \quad (5)$$

Since HSE calculations are computationally very demanding in particular for structural relaxations, we limit ourselves to HSE calculations using the experimental structure (i.e. lattice constants and atomic positions) (listed as HSE* in Table 2) for the formation enthalpy of the metal oxides. As an example, we compare in Table 2 a fully relaxed HSE calculation with one based on the experimental structure for TiO_2 and Ti_2O_3. For completeness we also added the (fully relaxed) PBE results. We notice that the fully relaxed and HSE based on the experimental structure agree within 0.5 % and are in good agreement with experiment. The corresponding values for $\Delta\mu_{\mathrm{Ti}}$ and $\Delta\mu_{\mathrm{O}}$ for both O-rich and Ti-rich conditions are listed in Table 2.

3 Results

3.1 Formation enthalpies & chemical potentials

The defect formation energy defined in Eq. (1) depends on the chemical potential of Ti, O and the TM impurities and Eqs. (3-5) provide the constraints on these chemical potentials. In this section we present the calculated formation enthalpies for the TM oxides and the limiting values for the chemical potentials. For each TM we considered several oxides with different stoichiometry as listed in Table 4. As explained in the previous section we use experimental lattice constants for the total energy calculations. In Table 3 we summarize these constants together with their PBE optimized values for the considered TM oxides. The calculated enthalpies of formation are listed in Table 4 together with the available experimental values. We notice that PBE and HSE calculations with the latter using the experimental structure yield similar results and the calculated values are in good agreement with the experimental ones (with the exception of VO).

Using these enthalpies of formation for various oxide materials, chemical potentials are computed and plotted in Fig. 1 for (a) group V-b within PBE, (b) group VI-b within PBE, (c) group V-b within HSE and (d) group VI-b within HSE. The chemical potential ranges are determined by $\Delta\mu_{\mathrm{O}} = 0$ (corresponding to O-rich conditions) and $\Delta\mu_{\mathrm{O}} = -3.80$ eV (PBE) or -4.11 eV (HSE), corresponding to Ti-rich conditions (i.e. O-poor conditions). In all cases (except Nb), we find that under Ti-rich conditions $\Delta\mu_{\mathrm{X}} = 0$, i.e. the chemical potential corresponds to that of the elemental solid phase of X (for all X). From Fig. 1 we see that, under oxygen-rich conditions, the chemical potentials for V, Nb and Ta are determined by V_2O_5, Nb_2O_5 and Ta_2O_5, respectively. For group VI-b elements, the chemical potentials for Cr, Mo and W are taken from CrO_2, MoO_3 and WO_3, respectively, for PBE, whereas they are taken from Cr_2O_3, MoO_3 and WO_3, respectively, for HSE.

Finally, the values of μ_{X} and μ_{O} used for the formation energy calculation under O-rich and Ti-rich conditions both within PBE and HSE are summarized in Table 5. These results will be used in the next section where we present the formation energies of the different TM impurity atoms.

3.2 Defect formation energies

To see whether a dopant can be easily incorporated into TiO_2 and act as a potential donor or acceptor of electrons, we have calculated the defect formation energies and the (thermodynamic) transition levels for TiO_2:X (X=V, Nb, Ta, Cr, Mo, W) with the HSE functional. The transition level $\varepsilon(q/q')$ between two charge states q and q' is defined as the Fermi energy at which $E^f(X^q) = E^f(X^{q'})$ i.e.

$$\varepsilon(q/q') = \frac{E^f(X^q; E_F = 0) - E^f(X^{q'}; E_F = 0)}{q' - q}. \quad (6)$$

When the Fermi level is below $\varepsilon(q/q')$ charge state q is stable, otherwise charge state q' is stable †. Shallow donor (acceptor) levels correspond to transition levels that lie within k_BT from the CBM (VBM), otherwise they are labelled as deep. The results are shown in Fig. 2. For a given value of the Fermi level only the lowest energy charge state is shown for each dopant.‡

The HSE results of Fig. 2 show that the transition levels $\varepsilon(+/0)$ for Nb and Ta are located in the conduction band i.e. for all Fermi level values in the band gap the preferred charge state is 1+, thereby demonstrating the shallow character of the donor impurities both providing one electron to the conduction band.[28,29] A similar result was obtained for TiO_2:Nb by Körner and Elsässer within a LDA+SIC approach.[18] The result is also in line with the metallic conductivity observed in TiO_2:Nb[4,5] and TiO_2:Ta[6,53]. Moreover a defect level of 20.79 meV below the CBM has been observed for TiO_2:Nb[54], which confirms the shallow behavior of the impurity. The formation energy of a charged Ta impurity is lower than that of a Nb one. This results in a higher concentration of the former, thereby favoring a higher conductivity for TiO_2:Ta, though the final value for the conductivity will also depend on other factors such as the presence of compensating native defects. A similar result was suggested on the basis of formation energy calculations of neutral impurities.[20] In contrast to Nb and Ta, sub-

† a charge state q refers to a state relative to Ti^{4+}

‡ For completeness we have tested the effect of spin-orbit coupling in the case of W using the PBE functional. As can be seen in Fig. 1, only WO_3 needs to be considered (oxygen rich conditions). Spin-orbit coupling lowers $\Delta H_f(\mathrm{WO_3})$ by ∼0.7 eV, so the W defect formation energies will rise by the same amount. Note, however that the transition levels do not depend on the chemical potentials.

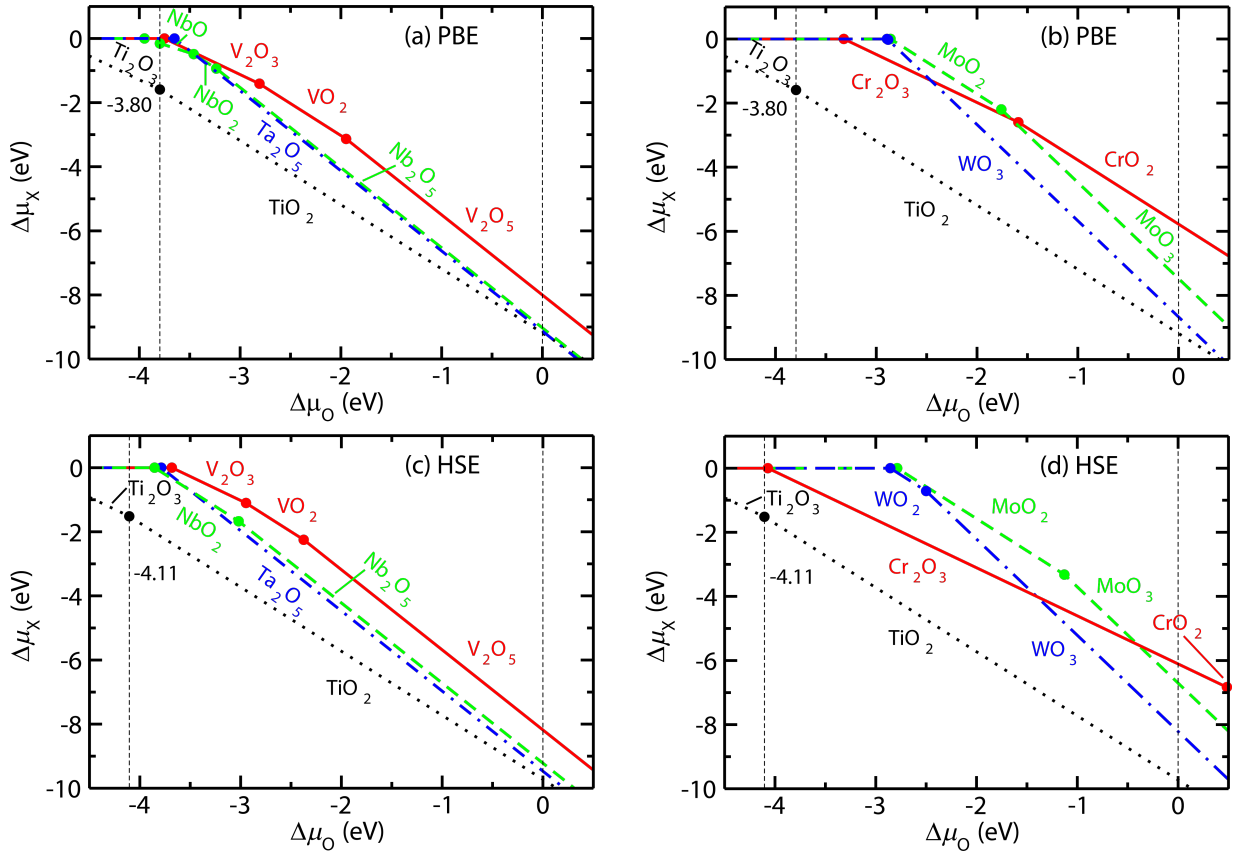

Fig. 1 Chemical potentials for group V-b (left side) and VI-b (right side) elements. The upper panels are calculated within PBE, whereas the lower panels are calculated within HSE. The vertical dashed line at $\Delta\mu_O = 0$ corresponds to O-rich conditions, while the other vertical dashed line at $\Delta\mu_O = -3.80$ eV (PBE) or -4.11 eV (HSE) corresponds to Ti-rich conditions.

Table 2 The enthalpies of formation for TiO_2 and Ti_2O_3 obtained by PBE and HSE and the experimental values.[41] The results obtained from a HSE calculation using the experimental structure (i.e. lattice constants and atomic positions) is given in the third line (HSE*). The corresponding values for $\Delta\mu_{Ti}$ and $\Delta\mu_O$ both in O-rich and Ti-rich conditions are also presented. Units are in eV.

			O-rich		Ti-rich	
	$\Delta H_f(TiO_2)$	$\Delta H_f(Ti_2O_3)$	$\Delta\mu_{Ti}$	$\Delta\mu_O$	$\Delta\mu_{Ti}$	$\Delta\mu_O$
PBE	−9.19	−14.58	−9.19	0	−1.59	−3.80
HSE	−9.73	−15.35	−9.73	0	−1.52	−4.11
HSE*	−9.72	−15.27	−9.72	0	−1.38	−4.17
Exp.	−9.73	−15.76				

Table 3 Experimental lattice constants used for the HSE energy calculations and the PBE optimized lattice constants. The values a, b and c are in Å and the values α, β and γ are in degrees.

	k-points	Space group (#)	Experiment	PBE
VO	$14\times14\times14$	$Fm\bar{3}m$ (225)	$a=4.062$ [a]	$a=4.191$
VO_2	$6\times6\times6$	$P4_2/mnm$ (136)	$a=4.5546, c=2.8514$ [b]	$a=4.614, c=2.799$
V_2O_3	$4\times4\times4$	$R\bar{3}c$ (167)	$a=4.952, c=14.002$ [c]	$a=4.809, c=14.438$
V_2O_5	$4\times4\times4$	$Pmmn$ (59)	$a=11.512, b=3.564, c=4.368$ [d]	$a=11.570, b=3.577, c=4.899$
V_6O_{13}	$4\times4\times4$	Pc (7)	$a=10.061, b=3.711, c=11.963$ [e]	$a=10.245, b=3.668, c=11.996$
			$\beta=100.93$	$\beta=101.01$
NbO	$12\times12\times12$	$Pm\bar{3}m$ (221)	$a=4.210$ [a]	$a=4.260$
NbO_2	$8\times8\times8$	$I4_1/a$ (88)	$a=13.71, c=5.985$ [a]	$a=13.936, c=6.091$
Nb_2O_5	$4\times4\times4$	$P2/m$ (10)	$a=21.153, b=3.8233, c=19.356$ [f]	$a=21.652, b=3.878, c=19.815$
			$\beta=119.80$	$\beta=119.86$
TaO	$14\times14\times14$	$Fm\bar{3}m$ (225)	$a=4.422$ [a]	$a=4.510$
Ta_2O_5	$8\times8\times8$	$P6/mmm$ (191)	$a=7.248, c=3.880$ [g]	$a=7.346, c=3.891$
CrO_2	$8\times8\times8$	$P4_2/mnm$ (136)	$a=4.421, c=2.917$ [h]	$a=4.456, c=2.934$
Cr_2O_3	$4\times4\times4$	$R\bar{3}c$ (167)	$a=4.961, c=13.599$ [c]	$a=4.949, c=13.846$
MoO_2	$8\times8\times8$	$P2_1/c$ (14)	$a=5.6109, b=4.8562, c=5.6285$ [i]	$a=5.639, b=4.919, c=5.694$
			$\beta=120.95$	$\beta=120.74$
MoO_3	$6\times6\times6$	$Pnma$ (62)	$a=3.9616, b=13.856, c=3.6978$ [j]	$a=3.973, b=16.815, c=3.705$
WO_2	$4\times4\times4$	$P2_1/c$ (14)	$a=5.563, b=4.896, c=5.663$ [k]	$a=5.620, b=4.952, c=5.724$
			$\beta=120.47$	$\beta=120.45$
WO_3	$4\times4\times4$	P_1 (2)	$a=7.313, b=7.525, c=7.690$ [l]	$a=7.508, b=7.663, c=7.822$
			$\alpha=88.847, \beta=90.912, \gamma=90.940$	$\alpha=89.4450, \beta=90.2957, \gamma=90.3133$

[a] Ref. 42, [b] Ref. 43, [c] Ref. 43, [d] Ref. 44, [e] Ref. 45, [f] Ref. 46, [g] Ref. 47, [h] Ref. 48, [i] Ref. 49, [j] Ref. 50, [k] Ref. 51, [l] Ref. 52

Table 4 Enthalpy of formation for various oxides obtained by a (fully relaxed) PBE and by an HSE calculation, with the latter using the experimental structure. Experimental values are also shown as a reference.[41] Units are in eV.

ΔH_f	PBE	HSE	Experiment
VO	−2.91	−2.95	−4.48
VO_2	−7.03	−7.00	−7.37
V_2O_3	−11.25	−11.04	−12.63
V_2O_5	−16.01	−16.37	−16.07
V_6O_{13}	−44.75	−45.27	−46.05
NbO	−3.95	−4.16	−4.35
NbO_2	−7.41	−7.71	−8.24
Nb_2O_5	−18.06	−18.44	−19.69
TaO	−1.82	−1.71	–
Ta_2O_5	−18.26	−18.94	−21.20
CrO_2	−5.78	−5.87	−6.20
Cr_2O_3	−9.97	−12.09	−11.76
MoO_2	−5.72	−5.58	−6.09
MoO_3	−7.48	−6.70	−7.72
WO_2	−5.79	−5.71	−6.11
WO_3	−8.67	−8.21	−8.74

stitutional V acts as a deep donor with the $\varepsilon(+/0)$ transition level at 1.59 eV below the HSE CBM (or 1.37 eV below the experimental CBM). This result is in line with x-ray absorption spectroscopy results[55] and EPR measurements[56] which show that vanadium is in the charge state "V^{4+}" (i.e. $q=0$ in our notation), which confirms its deep character as an electron donor. We also notice that resonant photoemission experiments on rutile TiO_2:V locate an occupied donor level 0.8 eV below the CBM (where the band gap value was taken as 3.0 eV).[57] Our calculations suggest that V demonstrates amphoteric behavior i.e. at Fermi level values close to the HSE CBM it turns into an acceptor with charge state $1-$. However, this is more likely to be an artefact resulting from the slight overestimation of the band gap by HSE. The results for Nb, Ta, and V are in line with those of ref. 17: our donor defect level for vanadium is somewhat larger (1.59 versus 1.36 eV) and our formation energies are in general somewhat smaller.

The values of the chemical potentials appearing in Eq. 1 reflect the influence of the experimental growth conditions. Using the values of Table 5 we consider two limiting cases in Fig. 2, namely, O rich and Ti rich (i.e. O poor). Comparing these conditions shows that Nb- and Ta-doping will be more effective under O-poor conditions i.e. under a reducing deposition atmosphere[21,53], whereas V doping is hardly affected by the experimental growth conditions. For completeness the PBE results are also given in Fig. 2. Although they give qualitatively the same result for the V-b TM atoms (using the PBE band gap), the V dopant turns out to be considerably more shallow than in the HSE case. One also observes that a straightforward use of the PBE transition energies with the experimental band gap does not lead to correct results, as expected, and a correction scheme should be invoked as in ref. 17.

Table 5 Calculated (both in PBE and HSE) values for $\Delta\mu_X$ and $\Delta\mu_O$ both in O-rich and Ti-rich conditions. Units are in eV.

	PBE				HSE			
	O-rich		Ti-rich		O-rich		Ti-rich	
X	$\Delta\mu_X$	$\Delta\mu_O$	$\Delta\mu_X$	$\Delta\mu_O$	$\Delta\mu_X$	$\Delta\mu_O$	$\Delta\mu_X$	$\Delta\mu_O$
V	−8.00	0	0	−3.80	−8.18	0	0	−4.11
Nb	−9.03	0	−0.15	−3.80	−9.22	0	−0.05	−4.11
Ta	−9.13	0	0	−3.80	−9.47	0	0	−4.11
Cr	−5.78	0	0	−3.80	−5.87	0	0	−4.11
Mo	−7.48	0	0	−3.80	−6.70	0	0	−4.11
W	−8.67	0	0	−3.80	−8.21	0	0	−4.11

In the case of W doping, the 2+ charge state has the lowest formation energy for Fermi energies between the VBM and the CBM, thereby demonstrating its shallow donor character, which is fully in agreement with the experimental observation that W doping drastically decreases the resistivity.[25,58] X-ray photoelectron spectroscopy (XPS) experiments indicate that 88% of the available W impurities donate two electrons to the TiO_2 host system, whereas for the other 12% the electron remains with the dopant atom.[25] However, despite the fact that W provides two rather than one electron, the observed conductivity of TiO_2:W is lower than that of TiO_2:Nb or TiO_2:Ta.[58] The considerable higher formation energy of the W 2+ state compared to the 1+ state of Nb or Ta at Fermi energies close to the CBM (a situation that corresponds to that of an n-doped system) is consistent with these experimental observations, though other factors such as the presence of electron trapping centers due to native defects (e.g. vacancies) can play an important role too.[58]

For Mo doping the situation is different from that of W. The 2+ state is stable for Fermi energies up to an energy of 0.68 eV below the HSE CBM (0.46 eV below the experimental CBM) from where the 1+ becomes stable. The HSE calculations subsequently predict a transition to the 1− charge state at 0.22 eV below the CBM. This shows that Mo is a so-called "negative U" impurity, where the neutral charge state is never stable and a donor turns into an acceptor depending on the Fermi energy.[28,29] However, due to the overestimation of the band gap by the HSE functional, the negative U behavior is likely to be an artefact. Therefore we consider Mo to be an electron donor, donating one or two electrons to TiO_2 depending on the actual value of the Fermi level, which is determined by the overall charge neutrality of the system (i.e. including charged native defects). This result is reminiscent of the experimental situation. An increased conductivity is observed in Mo-doped TiO_2 with the Mo impurity occuring in two charge states : 70% of the dopants has a charge state "Mo^{6+}" thereby donating two electrons and 30% has a charge state "Mo^{5+}" thereby donating one electron.[12,14,15] However, in ref. 59 only Mo^{5+} was observed. The existence of Mo^{5+} is often attributed to the presence of O vacancies, which indeed are known to act as shallow donors thereby moving the Fermi level towards the CBM[60], where Mo will act as a single electron donor. The VI-b impurity Cr is clearly amphoteric with a stable 2+ state for Fermi energies between the VBM and $E_F = E_v + 0.89$ eV and a stable 1− state from $E_F = E_v + 1.52$ eV to E_c, which makes it both a deep donor and a deep acceptor. Since as-grown TiO_2 behaves as an n-type semiconductor due to intrinsic defects acting as donor dopants (e.g. oxygen vacancies)[60,61], the actual Fermi level is lying close to the CBM. Our calculations show that for those Fermi energies Cr dopants act as acceptors. This can explain the observed reduction of the conductivity in Cr-doped TiO_2.[62,63] In ref. 63 amphoteric behavior is observed in rutile TiO_2:Cr with a change in the oxidation state of Cr from Cr^{3+} to Cr^{6+} in going from a strongly reducing regime towards a more oxidizing regime. In the former case Cr acts as an acceptor accepting one electron ($Cr^{4+} \rightarrow Cr^{3+}$) whereas in the latter case it donates two electrons ($Cr^{4+} \rightarrow Cr^{6+}$). Although our calculations focus on anatase TiO_2 (not on rutile) and do not consider any concomitant effects from native defects, it is remarkable that our calculations yield the same conclusion. According to Mizushima et al.[64] the Cr^{3+}, and thus the acceptor level, is 2.7 eV below the (rutile) conduction band, which confirms the deep character of the impurity level in TiO_2. From Fig. 2 it follows that growth conditions hardly affect the formation energy of W, but O-rich conditions are preferred for both Mo and Cr dopants. For Cr the formation energy drastically decreases under O-rich conditions. A similar effect is observed for the formation energy of Mo, which is higher than that of W under O-poor conditions but which becomes comparable to or is even lower than that of W under O-rich conditions. As a reference we also included the bare PBE results (i.e. without additional band gap corrections) in Fig. 2. For W and Cr PBE yields qualitatively similar results to HSE, but Mo would emerge as a shallow donor providing two electrons per atom. The transition level positions that appear within the (calculated) band gap in for V, Cr and Mo are summarized in Table 6 for both HSE and PBE.

Table 6 Calculated (in both PBE and HSE) transition level positions for dopant X with respect to the VBM. Units are in eV.

X	q/q'	$\varepsilon(q/q')$ (PBE)	$\varepsilon(q/q')$ (HSE)
V	$(+/0)$	1.81	2.03
	$(0/-)$		3.57
Cr	$(2+/0)$		0.89
	$(2+/+)$	0.94	
	$(+/0)$	0.98	
	$(0/-)$	1.27	1.52
Mo	$(2+/+)$		2.94
	$(+/-)$		3.40

4 Conclusions

In this work we have identified the electronic nature of group V-b (V, Nb, Ta) and group VI-b (Cr, Mo, W) impurities in TiO_2 combining thermodynamics and first-principles calculations. The defect formation energy for different charge states of the impurity was calculated taking into account the impurity solubility limit

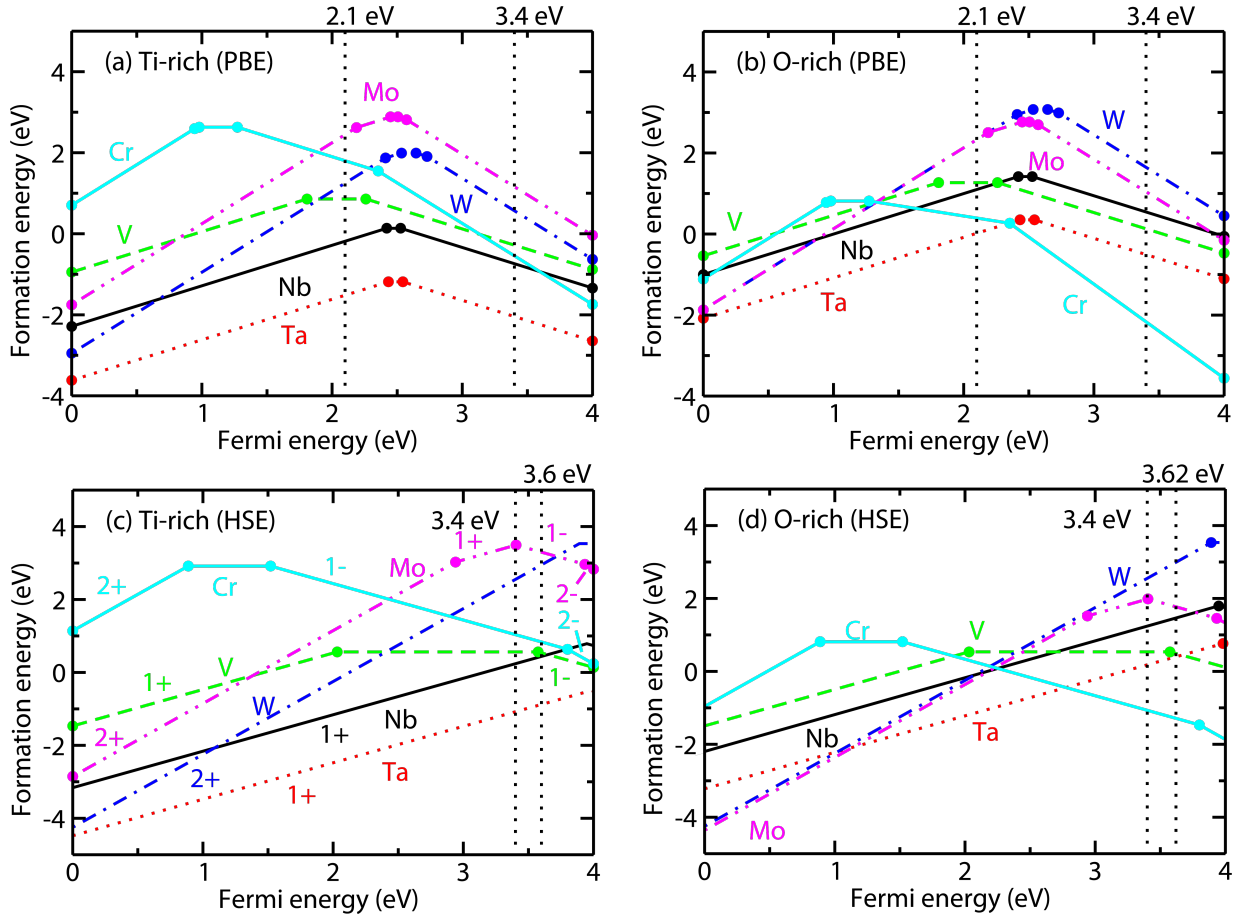

Fig. 2 Formation energies for TiO_2:X (X=V, Nb, Ta, Cr, Mo, W) under Ti-rich (left) and O-rich (right) conditions calculated by PBE (top) and HSE (bottom). The slope of the lines is given by the charge state. For the HSE result in Ti-rich conditions the charge state is explicitly indicated for convenience. The vertical dotted bars denote the band gap positions (experimental band gap at 3.4 eV, PBE band gap at 2.1 eV and HSE band gap at 3.62 eV). Only the lowest energy charge states are plotted and the transition levels are marked by filled circles.

and the stability of TiO_2. Since reliable defect formation energies depend on accurate band gap values we used the HSE06 hybrid functional, which has proven to provide realistic defect formation energies for charged impurities. All of the obtained results are in agreement with the experimental observations. Nb, Ta, W and Mo are identified as shallow donors with W providing two electrons but with a considerable higher formation energy than Nb and Ta that each donate one electron. The lowest formation energy of the studied impurities is obtained for Ta. Mo is a shallow donor donating one electron to TiO_2 but a slight shift of the Fermi energy towards lower values (e.g. through the presence of compensating acceptors) would turn Mo into a double donor. V acts as a deep donor and Cr is amphoteric acting as a donor or an acceptor depending on the actual value of the Fermi energy and thus will act as an electron trapping center in n-type as-grown TiO_2.

5 Acknowledgments

We gratefully acknowledge financial support from the IWT-Vlaanderen through the ISIMADE project, the FWO-Vlaanderen through projects G.0191.08 and G.0150.13, and the BOF-NOI of the University of Antwerp. This work was carried out using the HPC infrastructure of the University of Antwerp (CalcUA) a division of the Flemish Supercomputer Center VSC, which is funded by the Hercules foundation. M. M. acknowledges financial support from the GOA project "XANES meets ELNES" of the University of Antwerp.

References

1 K. Hashimoto, H. Irie and A. Fujishima, *Jpn. J. Appl. Phys.*, 2005, **44**, 8269.

2 F. Gracia, J. P. Holgado, A. Caballero and A. R. Gonzalez-Elipe, *J. Phys. Chem. B*, 2004, **108**, 17466.

3 H. Tang, F. Lévy, H. Berger and P. E. Schmid, *Phys. Rev. B*, 1995, **52**, 7771.

4 Y. Furubayashi, T. Hitosugi, Y. Yamamoto, K. Inaba, G. Kinoda, Y. Hirose, T. Shimada and T. Hasegawa, *Appl. Phys. Lett.*, 2005, **86**, 252101.

5 Y. Furubayashi, T. Hitosugi, Y. Yamamoto, Y. Hirose, G. Kinoda, K. Inaba, T. Shimada and T. Hasegawa, *Thin Solid Films*, 2006, **496**, 157.

6 T. Hitosugi, Y. Furubayashi, A. Ueda, K. Itabashi, K. Inaba, Y. Hirose, G. Kinoda, Y. Yamamoto, T. Shimada and T. Hasegawa, *Jpn. J. Appl. Phys.*, 2005, **44**, L1063.

7 S. Sathasivam, D. S. Bhachu, Y. Lu, N. Chadwick, S. A. Althabaiti, A. O. Alyoubi, S. N. Basahel, C. J. Carmalt and I. P. Parkin, *Sci. Rep.*, 2015, **5**, 10952.

8 Y. Matsumoto, M. Murakami, T. Shono, T. Hasegawa, T. Fukumura, M. Kawasaki, P. Ahmet, T. Chikyow, S.-y. Koshihara and H. Koinuma, *Science*, 2001, **291**, 854.

9 R. Janisch and N. A. Spaldin, *Phys. Rev. B*, 2006, **73**, 035201.

10 N. H. Hong, J. Sakai and A. Hassini, *Appl. Phys. Lett.*, 2004, **84**, 2602.

11 T. Droubay, S. M. Heald, V. Shutthanandan, S. Thevuthasan, S. A. Chambers and J. Osterwalder, *J. Appl. Phys.*, 2005, **97**, 046103.

12 V. Stengl and S. Bakardjieva, *J. Phys. Chem. C*, 2010, **114**, 19308.

13 M. Khan, J. Xu, W. Cao and Z.-K. Liu, *J. Nanosci. Nanotechnol.*, 2014, **14**, 6865.

14 S. Wang, L. N. Bai, H. M. Sun, Q. Jiang and J. S. Lian, *Powder Technol.*, 2013, **244**, 9.

15 B. Houng, C. C. Liu and M. T. Hung, *Ceram. Int.*, 2013, **39**, 3669.

16 B. J. Morgan, D. O. Scanlon and G. W. Watson, *J. Mater. Chem.*, 2009, **19**, 5175.

17 J. Osorio-Guillén, S. Lany and A. Zunger, *Phys. Rev. Lett.*, 2008, **100**, 036601.

18 W. Körner and C. Elsässer, *Phys. Rev. B*, 2011, **83**, 205315.

19 P. Deák, B. Aradi and T. Frauenheim, *Phys. Rev. B*, 2011, **83**, 155207.

20 H. A. Huy, B. Aradi, T. Frauenheim and P. Deák, *J. Appl. Phys.*, 2012, **112**, 016103.

21 H.-Y. Lee and J. Robertson, *J. Appl. Phys.*, 2013, **113**, 213706.

22 V. Çelik and E. Mete, *Phys. Rev. B*, 2012, **86**, 205112.

23 R. Long and N. J. English, *Chem. Phys. Lett.*, 2011, **513**, 218.

24 R. Long and N. J. English, *Phys. Rev. B*, 2011, **83**, 155209.

25 D.-M. Chen, G. Xu, L. Miao, L.-H. Chen, S. Nakao and P. Jin, *J. Appl. Phys.*, 2010, **107**, 063707.

26 H. Kamisaka, T. Hitosugi, T. Suenaga, T. Hasegawa and K. Yamashita, *J. Chem. Phys.*, 2009, **131**, 034702.

27 J. Pan, C. Li, Y. Zhao, R. Liu, Y. Gong, L. Niu, X. Liu and B. Chi, *Chem. Phys. Lett.*, 2015, **628**, 43.

28 C. Freysoldt, B. Grabowski, T. Hickel, J. Neugebauer, G. Kresse, A. Janotti and C. G. Van de Walle, *Rev. Mod. Phys.*, 2014, **86**, 253.

29 C. G. Van de Walle and J. Neugebauer, *J. Appl. Phys.*, 2004, **95**, 3851.

30 J. Heyd, G. E. Scuseria and M. Ernzerhof, *J. Chem. Phys.*, 2003, **118**, 8207.

31 J. Heyd, G. E. Scuseria and M. Ernzerhof, *J. Chem. Phys.*, 2006, **124**, 219906.

32 G. Kresse and J. Furthmüller, *Phys. Rev. B*, 1996, **54**, 11169.

33 G. Kresse and D. Joubert, *Phys. Rev. B*, 1999, **59**, 1758.

34 J. P. Perdew, K. Burke and M. Ernzerhof, *Phys. Rev. Lett.*, 1996, **77**, 3865.

35 J. K. Burdett, T. Hughbanks, G. J. Miller, J. W. Richardson Jr. and J. V. Smith, *J. Am. Chem. Soc.*, 1987, **109**, 3639.

36 R. Saniz, Y. Xu, M. Matsubara, M. Amini, H. Dixit, D. Lamoen and B. Partoens, *J. Phys. Chem. Solids*, 2013, **74**, 45.

37 R. Rurali and X. Cartoixá, *Nano Lett.*, 2009, **9**, 975.

38 Y. Kumagai and F. Oba, *Phys. Rev. B*, 2014, **89**, 195205.

39 G. Petretto and F. Bruneval, *Phys. Rev. Appl.*, 2014, **1**, 024005.

40 R. J. Gonzalez, R. Zallen and H. Berger, *Phys. Rev. B*, 1997, **55**, 7014.

41 J. M. W. Chase, *J. Phys. Chem. Ref. Data Monograph No. 9 NIST. JANAF Thermochemical Tables (1998) 1925.*, 1998, **9**, 1.

42 R. Wyckoff, *Crystal Structures*, Wiley, 1963.

43 R. E. Newnham and Y. M. de Haan, *Z. Kristallogr. - Cryst. Mater.*, 1962, **117**, 235.

44 R. Enjalbert and J. Galy, *Acta Crystallogr., Sect. C*, 1986, **42**, 1467.

45 J. Höwing, T. Gustafsson and J. O. Thomas, *Acta Crystallogr., Sect. B*, 2003, **59**, 747.

46 K. Kato, *Acta Crystallogr., Sect. B*, 1976, **32**, 764.

47 N. Terao, *Jpn. J. Appl. Phys.*, 1967, **6**, 21.

48 W. H. Baur and A. A. Khan, *Acta Crystallogr., Sect. B*, 1971, **27**, 2133.

49 B. G. Brandt and A. C. Skapski, *Acta Chem. Scand.*, 1967, **21**, 661.

50 H. Sitepu, B. H. O'Connor and D. Li, *J. Appl. Crystallogr.*, 2005, **38**, 158.

51 N. Jiang and J. C. H. Spence, *Phys. Rev. B*, 2004, **70**, 245117.

52 P. Woodward, A. Sleight and T. Vogt, *J. Phys. Chem. Solids*, 1995, **56**, 1305.

53 P. Mazzolini, P. Gondoni, V. Russo, D. Chrastina, C. S. Casari and A. L. Bassi, *J. Phys. Chem. C*, 2015, **119**, 6988.

54 H. Bae, J.-S. Ha, S. Park, T. Chikyow, J. Chang and D. Oh, *J. Vac. Sci. Technol., B*, 2012, **30**, 050603.

55 G. Rossi, M. Calizzi, V. D. Cintio, S. Magkos, L. Amidani, L. Pasquini and F. Boscherini, *J. Phys. Chem. C*, 2016, **120**, 7457.

56 B. Tian, C. Li, F. Gu, H. Jiang, Y. Hu and J. Zhang, *Chem. Eng. J.*, 2009, **151**, 220.

57 D. Morris and R. Egdell, *J. Mater. Chem.*, 2001, **11**, 3207.

58 U. Takeuchi, A. Chikamatsu, T. Hitosugi, H. Kumigashira, M. Oshima, Y. Hirose, T. Shimada and T. Hasegawa, *J. Appl. Phys.*, 2010, **107**, 023705.

59 D. Mardare, N. Cornei, D. Luca, M. Dobromir, S. A. Irimiciuc, L. Punga, A. Pui and C. Adomnitei, *J. Appl. Phys.*, 2014, **115**, 213501.

60 A. Janotti, J. B. Varley, P. Rinke, N. Umezawa, G. Kresse and C. G. Van de Walle, *Phys. Rev. B*, 2010, **81**, 085212.

61 U. Diebold, *Surf. Sci. Rep.*, 2003, **48**, 53.

62 J.-M. Herrmann, *New J. Chem.*, 2012, **36**, 883.

63 J. Nowotny, W. Macyk, E. Wachsman and K. A. Rahman, *J. Phys. Chem. C*, 2016, **120**, 3221.

64 K. Mizushima, M. Tanaka, A. Asai, S. Iida and J. B. Goodenough, *J. Phys. Chem. Solids*, 1979, **40**, 1129.